2007 Davisson–Germer prize lecture

Low-dimensional electron gas at semiconductor surfaces

I. Barke[a], R. Bennewitz[a], J.N. Crain[a], S.C. Erwin[b], A. Kirakosian[a], J.L. McChesney[a], F.J. Himpsel[a,*,1]

[a] *Department of Physics, UW-Madison, 1150 University Ave., Madison, WI 53706, United States*
[b] *Naval Research Laboratory, Washington DC 20375, United States*

Abstract

In recent years, it has become possible to create well-ordered semiconductor surfaces with metallic surface states by using self-assembly of metal atoms. Since these states lie in the band gap of the semiconductor, they completely decouple from the substrate. In addition to two-dimensional structures it is possible to obtain arrays of one-dimensional atomic chains, which may be viewed as the ultimate nanowires. The dimensionality can be varied systematically by using vicinal surfaces with variable step spacing. Angle-resolved photoemission and scanning tunnelling spectroscopy reveal surprising features, such as a fractional band filling, nanoscale phase separation into doped and undoped chain segments, and a spin-splitting at a non-magnetic surface. Prospects for one-dimensional electron gas physics in atomic chains are discussed.
© 2007 Elsevier Ltd. All rights reserved.

1. The electron gas in low dimensions

The two-dimensional electron gas at semiconductor hetero-junctions has produced an enormous amount of interesting new physics [1–5]. Highlights are the integer and fractional quantum Hall effect, where electrons and magnetic flux quanta combine into a fascinating variety of composite particles. In the following, a different type of electron gas will be presented, which is created by a metallic surface state on a semiconductor [6–8]. Fig. 1 compares these electronic systems. The traditional electron gas consists of electrons in a quantum well state, whose envelope function extends over many lattice planes (Fig. 1 top). A surface state on a semiconductor is concentrated within a single atomic spacing, due to the localized nature of broken covalent bonds (Fig. 1 bottom). The single most important parameter characterizing an electron gas is the electron density, and in this respect the two electron gases differ by several orders of magnitude. The electron density of a doped surface state can be as

high as 10^{14} e$^-$/cm^2 (corresponding to 1/7 of a Si(111) mono-layer of dopants), while a typical electron density for the quantum Hall effect is only 10^{11} e$^-$/cm^2. The three-dimensional electron densities differ even more, since the surface state wave function is compressed to a monolayer. As a consequence of the higher electron density, the kinetic energy scale moves up from meV in the quantum Hall effect to eV for a surface state. That makes it possible to explore the electron gas in a completely different regime.

One might suspect that the increase in density makes the electron gas more free-electron-like, since the kinetic energy increases faster than the Coulomb repulsion. However, the broken bond orbitals are localized not only perpendicular to the surface, but also laterally. Therefore, the Coulomb repulsion U_C for placing two electrons in the same orbital increases dramatically compared to the Coulomb repulsion between adjacent electrons in a Wigner crystal. For Si adatoms on the Si(111) 7 × 7 surface, a splitting $U_C \approx 0.2$ eV between the upper and lower Hubbard band has been predicted [9]. So far, it could not be resolved experimentally due to a competing electron–phonon interaction involving a 70 meV surface phonon [10]. Comparing the experimental upper limit

* Corresponding author. Tel.: +1 608 263 5590; fax: +1 608 265 2334.
E-mail address: fhimpsel@facstaff.wisc.edu (F.J. Himpsel).
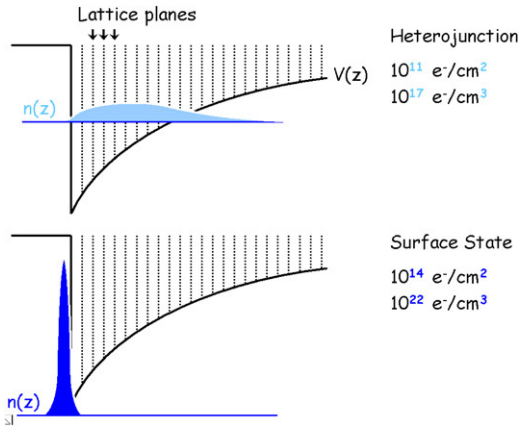1 Recipient of the 2007 Davisson–Germer Prize of the APS.

Fig. 1. Comparison of two versions of the two-dimensional electron gas: Top: A quantum well state at a semiconductor heterojunction Bottom: A metallic surface state at a semiconductor surface (bottom). The surface state has much higher electron density.

$U_C \leq 0.1$ eV to the band width $W \approx 0.3$ eV [10], one expects correlation effects to be small. For Si adatoms on a SiC surface, however, the splitting between the Hubbard bands increases to $U_C \approx 2$ eV and the band width shrinks somewhat to $W \approx 0.2$ eV, as observed by a combination of photoemission [11], inverse photoemission [12], and scanning tunnelling spectroscopy [13]. Such a large U_C/W ratio triggers a transition to a Mott insulator. The increase of U_C in SiC can be rationalized by reduced dielectric screening and by a stronger localization of the Si3p bond orbitals. Other localized orbitals might increase U_C in similar fashion, such as the d-orbitals in transition and noble metals (compare the high temperature superconductors).

A one-dimensional electron gas can be created from a two-dimensional electron gas at a cleaved or gated heterojunction [14,15]. At a stepped semiconductor surface, it is possible to produce atomic chains by self-assembly of metal atoms (for an overview see [16]). These may be viewed as the ultimate nanowires. By increasing the chain spacing, one can reduce the dimensionality gradually from 2D to almost 1D. One-dimensional electrons are particularly interesting for theorists [17]. This is the lowest dimension that still allows for translational motion. Therefore it may be viewed as the lowest non-trivial dimension. Nevertheless, the interaction of electrons is far from trivial. In fact, electrons interact so strongly in one dimension that the single-electron concept breaks down and gives way to collective excitations. This becomes clear by realizing that electrons are unable to avoid each other when moving along the same one-dimensional line (Fig. 2a from [17]). A single excited electron causes a domino effect that excites all other electrons. Theoretical predictions call for a second phenomenon in 1D that is even more exotic: The hole created during a photoemission experiment decomposes into two collective excitations, the holon and spinon. The holon carries the charge of the hole but is spinless, while the spin is carried by the spinon. Holon and spinon have different group velocities (different slopes in Fig. 2(b)), which leads to the separation of spin and charge (for a quantitative calculation see [18]). This highly counter-intuitive result can
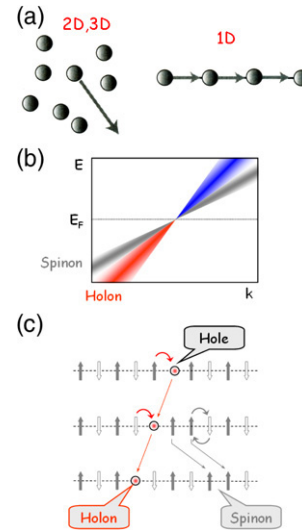

Fig. 2. Visualization of special electronic features in one-dimensional (1D) systems: (a) Electrons are able to avoid each other in higher dimensions (2D, 3D), which explains the single-particle character of the Fermi liquid. In 1D they move along the same line and interact strongly. As a result, only collective excitations survive (from [17], Fig. 1.3). (b) Schematic $E(k)$ band dispersion characterizing a 1D electron gas in reciprocal space, using the Tomonaga–Luttinger model for delocalized electrons (compare the calculation in [18]). Instead of a single band crossing the Fermi level E_F, one has two collective excitations with different group velocities, the holon and the spinon. The holon carries the positive charge of the hole that is left behind after photoemission, the spinon carries the spin of the hole. (c) Real space visualizaion of the separation of a hole into a holon and a spinon, using a half-filled Hubbard model for localized electrons. The propagation of holon and spinon is governed by two different processes (curved arrows), which lead to different velocities (compare [17], Fig. 3.4). (For interpretation of the references to colour in this figure legend, the reader is referred to the web version of this article.)

be visualized by going from reciprocal space in Fig. 2(b) to real space in Fig. 2(c). At the same time, delocalized electrons are traded for localized electrons by going from the Tomonaga–Luttinger model to the half-filled Hubbard model. It contains singly-occupied orbitals with antiferromagnetic order. A hole in the top row of Fig. 2(c) separates into a holon and a spinon in subsequent rows via hopping of electrons into empty sites (curved red arrows). The holon is an unoccupied site between opposite spins, and the spinon corresponds to a pair of adjacent parallel spins, i.e., an antiferromagnetic domain boundary. While the holon propagates by this hopping process, the spinon moves by an exchange between adjacent spins (pair of grey arrows). These two mechanisms explain the two different velocities of holon and spinon. As the holon and spinon approach the Fermi level, they become narrower and eventually converge to the same Fermi wave vector. The excitation energy vanishes right at the Fermi level, causing holon and spinon to recombine into a normal hole.

2. Metallic surface structures on semiconductors

Creating metallic surface states at semiconductors surfaces has been more difficult than anticipated. Many attempts to metallize semiconductor surfaces with alkali metals have been unsuccessful, even with an odd number of electrons per unit
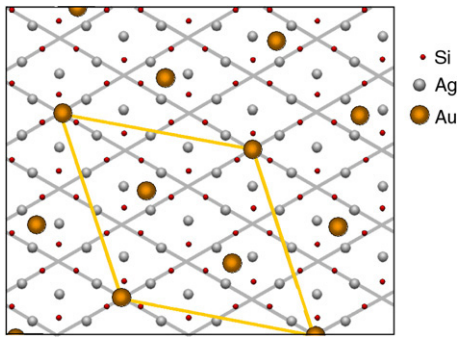
Fig. 3. Schematic of the metallic surfaces produced by adsorption of Ag and Au on Si(111). Exactly one monolayer of Ag creates a semiconducting $\sqrt{3} \times \sqrt{3}$ structure consisting of Ag trimers. Additional Ag or Au atoms adsorb on top of the trimers and act as surface dopants. The highest dopant concentration leads to an ordered $\sqrt{21} \times \sqrt{21}$ structure with 3 dopant atoms per unit cell. (For interpretation of the references to colour in this figure legend, the reader is referred to the web version of this article.)
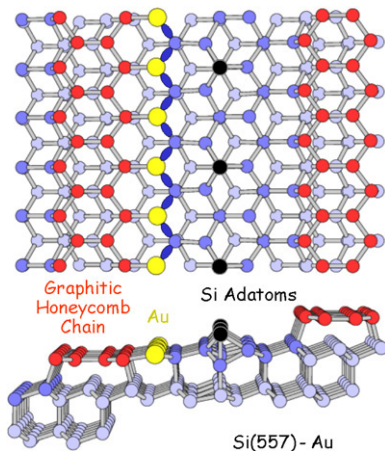

Fig. 4. Structural elements of Au-induced chain structures on stepped Si(111) surfaces, obtained from total energy calculations [45,53,54] and x-ray diffraction [42]. These structures are driven one-dimensional by the honeycomb chain, a narrow ribbon of graphitic Si (red). A chain of Au atoms is located at the center of the terrace in substitutional sites, contrary to expectations from step flow growth. The dark blue zig-zag chain of Si bonds pointing towards the Au atoms is associated with the spin-split, half-filled surface band discussed in Figs. 9 and 10. (For interpretation of the references to colour in this figure legend, the reader is referred to the web version of this article.)

cell. The reason is the localized nature of broken bonds at semiconductor surfaces, which leads to a large onsite Coulomb interaction U_C and a Hubbard gap. In recent years, the preparation of tailored semiconductor surfaces by self-assembly of metal atoms has made great progress, particularly on silicon. As a result, we have now several classes of metallic surfaces on semiconductors, both two-dimensional and one-dimensional. Typical surface structures are shown in Figs. 3 and 4 for the two cases. In the following, we will focus on metallic surface states of Si(111) and its vicinal surfaces:

2.1. Two-dimensional metallic surfaces

A particularly flexible class of two-dimensional, metallic surface structures are doped versions of the Si(111) $\sqrt{3} \times \sqrt{3}$-Ag structure with monovalent metal atoms as dopants,

(for example Ag, Au, and alkali metals [6–8,19–22]). The undoped Si(111) $\sqrt{3} \times \sqrt{3}$-Ag surface contains exactly one monolayer of Ag atoms (in units of Si(111) monolayers). These form a trimer structure, which is shown schematically in Fig. 3 (omitting smaller distortions that reduce the symmetry). Additional dopant atoms choose the site atop the centre of a trimer, as shown in Fig. 3 for Au atoms. They can be incorporated up to a maximum of 1/7 of a monolayer, where an additional $\sqrt{21} \times \sqrt{21}$ superlattice (orange lines) is formed on top of the $\sqrt{3} \times \sqrt{3}$ superlattice (grey lines). This coverage corresponds to three atoms in the $\sqrt{21} \times \sqrt{21}$ unit cell, which are shown in a symmetrical configuration in Fig. 3. The real arrangement has not been settled yet. There is a semiconducting surface state associated with the undoped $\sqrt{3} \times \sqrt{3}$ structure, whose band gap is smaller than that of bulk Si [19,23–25]. Additional monovalent atoms dope the conduction band of the surface state and create a metallic surface already at the lowest controllable dopant concentration of 1/1000 of a monolayer (compare Fig. 2 in [8]). These metallic states will be discussed in Section 3.1.

The closest analogue to the traditional semiconductor heterojunctions are quantum well states at the surface of In-based III–V compounds, where the Fermi level is pinned inside the conduction band [26,27]. Indium also introduces two- and one-dimensional surface states on Si(111), which have been the subject of intense study [28–30]. These are similar to the Ag- and Au-induced surface states discussed here.

2.2. One-dimensional atom chains

While Ag and Au form two-dimensional lattices on Si(111) at monolayer coverage and above, they change over to one-dimensional chain structures below about half a monolayer. The three-fold symmetry of the (111) surface is broken and gives way to three domains with chains oriented 120° apart. This set of chain structures can be extended greatly by using stepped Si(111) surfaces as templates [16,31–37]. A structural model characteristic of such chain structures is shown in Fig. 4.

The Si(111) 7×7 surface and its vicinal versions are suited particularly well for producing highly-perfect step arrays. Steps become very straight with such a large unit cell, because the formation of a kink requires adding $2 \times 7 = 14$ rows (one 7×7 unit cell, two layers deep). As a result, atomically straight step edges with a length of 20 000 edge atoms have been achieved on vicinal Si(111) 7×7 using a simple sequence of anneals [32, 33]. This requires a very accurate azimuthal cut of the Si wafer. The length of kink-free terraces can be extended to about 1 μm by heating the wafer with DC current parallel to the steps and keeping it strain-free during heating. Electromigration sweeps out the kinks and causes them to bunch into large facets [34,35].

The step spacing can be controlled by the step-step interaction via strain field [31]. A repulsive step-step interaction favours equispaced steps. The steps need to be spaced together closely to provide an interaction large enough for an atomically-perfect step spacing. This happens for vicinal Si(111) at a step spacing of about 6 nm, as shown in the top panel of Fig. 5 (from [36]). This Si(557) 3×1 surface structure consists of
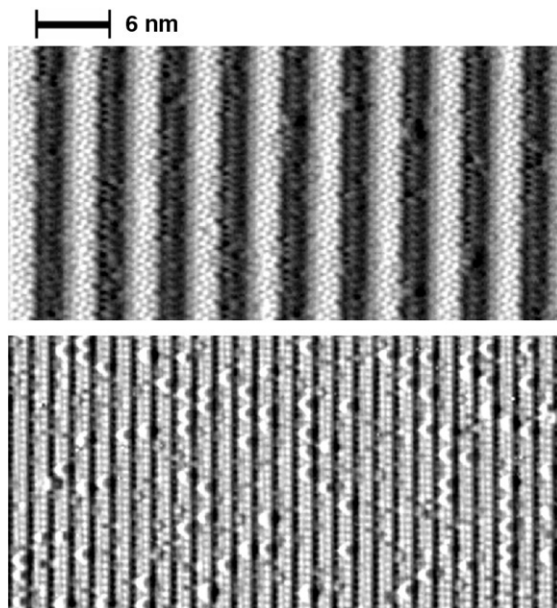
Fig. 5. Formation of atomic chains on a stepped Si(111) surface after depositing a sub-monolayer of Au. The 7×7 facets of the clean Si(557) surface (top, [36]) are broken up into double chains (bottom, [41]). This STM image shows the horizontal derivative of the height, giving the impression of illumination from the left.

a triple step and a terrace containing a single 7×7 unit cell. It has atomically-perfect periodicity, and the period of this atomic scale grating is known very accurately since the lattice constant of Si is a secondary length standard.

Stepped surfaces can be converted into atomic chain structures by depositing a sub-monolayer of metal atoms, most notably gold [16,37–55]. Vicinal Si(111) surfaces with all-odd Miller indices tend to form well-defined chain structures, and they are all metallic. An example is shown in the bottom panel of Fig. 5 (from [41]), where the clean Si(557) 3×1 surface in the top panel is converted to a chain structure by 1/5 of a monolayer of Au. The Au coverage is a critical parameter in obtaining highly-ordered chain structures, since surfaces with excess or insufficient Au coverage form patches of other structures. Atom chains are formed on vicinal Si(111) for a large group of metal atoms (alkalis, alkaline earths, In, Ag, Au, Pt, rare earths). These comprise valence states from 1 to 3, s-, p-, d-, and f-electrons, and magnetic atoms. Even the flat Si(111) surface forms one-dimensional chain structures with three domains. A single domain can be selected by choosing surface 1°–2° away from (111) with the steps parallel to the chains. An example is shown in Fig. 6 for Si(111) 5×2-Au. Apart from the Si(111) surface, which has the advantage of the large 7×7 unit cell, there are several other semiconductor surfaces supporting atomic chains, for example Si(100), Ge(100), SiC(100), and GaAs(110). Not all of these surfaces are metallic, but all the Au and In induced chains on vicinal and flat Si(111) surfaces are metallic at room temperature.

There is a common structural feature that appears to drive vicinal Si(111) and even flat Si(111) to become one-dimensional. Total energy calculations for chain structures induced by alkalis, alkaline earths, and noble metals suggest
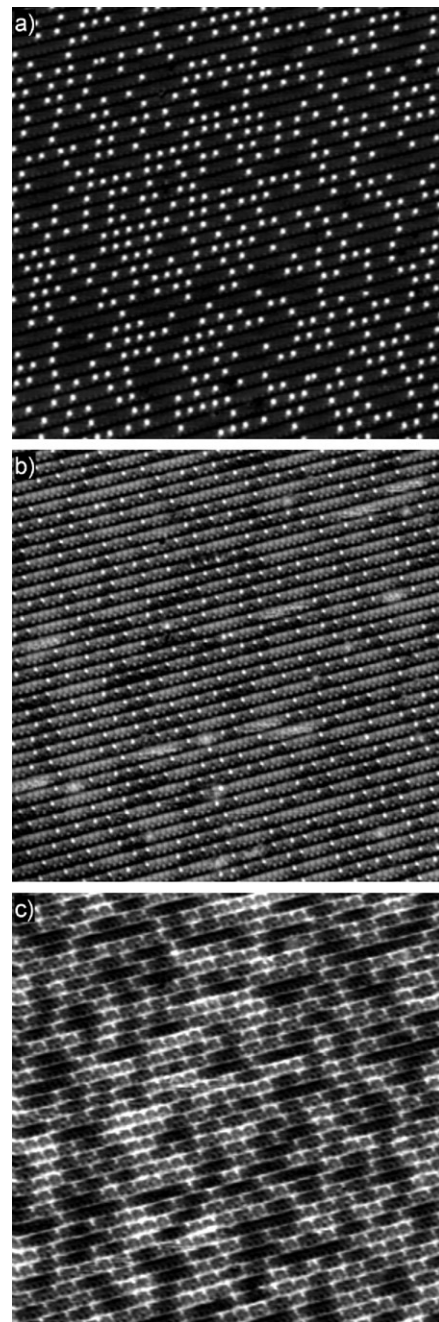

Fig. 6. The Si(111) 5×2-Au chain structure, which exhibits a large amount of extra Si dopants on top of the chains (1/40 of a monolayer). They are bunched into short sections with 5×4 periodicity, which alternate with empty sections. This pattern may be viewed as a one-dimensional version of stripes, which have been observed in the two-dimensional electron gas [5] and in cuprates. (a) Topography of a 50×50 nm region at a sample bias of -1.2 V, showing the dopant atoms. (b) Topography of the same region at $+0.8$ V sample bias, showing the underlying 5×2 chains. (c) dI/dV image at $+0.8$ V sample bias, showing different density of states in doped and undoped regions.

a common feature, the honeycomb chain [45,52–55]. This is a graphitic ribbon of Si atoms less than two hexagons wide but hundreds of nanometers long. It exhibits nearly perfect lattice match to Si(111) along the step direction, and very poor lattice match perpendicular to it, which gives it such an extremely high aspect ratio. The honeycomb chain resembles the graphene

ribbons which have attracted interest recently [56]. Bulk silicon avoids π-bonding, but it is quite common at silicon surfaces, where broken bonds are desperate for rebonding, for example, in the π-bonded chain of the Si(111) 2×1 cleavage surface and at the π-bonded dimers of the Si(100)2×1 surface.

The metal atoms seem to play a secondary role in forming the honeycomb chain, since many different metals have a similar effect. They might be useful for releasing surface strain by bridging the gap between the graphitic part and the rest of the Si(111) surface, or they may act as catalysts, similar to the role of transition metals in the formation of carbon nanotubes.

Fig. 4 demonstrates the key structural elements of the chain structures, using the Si(557)-Au structure as example. This model is obtained from a combination of surface x-ray diffraction [42] and total energy calculations [45,53,54]. The Au atom chains are located at the center of the terrace. They substitute for Si atoms in the outermost layer and become rigidly anchored to three Si atoms underneath. As a result, the Au chain is barely influenced by a possible reconstruction at the step edge or by the Si adatoms that double the unit cell. Naively one would expect the Au atoms to attach themselves to the step edge, where they find high coordination sites. This is just one of the many surprises delivered by these one-dimensional structures.

A second counter-intuitive feature of chain structures on vicinal Si(111) is the identity of the atom chains observed by STM. They originate from Si atoms with broken bonds, not from the Au atoms deposited on the surface. The Au atoms pair their s,p-electron with a neighboring Si bond and create a bound state well below E_F, according to first principles calculations [53]. That is in line with the high electronegativity of Au, which is higher than that of Si. The half-filled metallic bands observed by photoemission at these surfaces have mainly Si broken bond character. Thus, one may view the role of the Au atoms more as bystander and catalyst, while the Si broken bond orbitals form the electronically active wires.

3. Electronic states from angle-resolved photoemission

The most complete technique for mapping the electronic states at surfaces is angle-resolved photoemission [57–59]. It is able to measure the complete set of quantum numbers of surface electrons, most notably their energy E and momentum $\mathbf{p} = \hbar\mathbf{k}$, which consists of the two in-plane components k_x (along the chains) and k_y (perpendicular to the chains). Photoemission is even able to go beyond quantum numbers by analysing the line shape. For example, the line width provides the imaginary part of the self-energy Σ, and the difference between the peak positions of the dressed and bare bands gives the real part of Σ. These phenomena are just beginning to be addressed for semiconductor surfaces, for example in the electron–phonon interaction at the Si(111) 7×7 surface [10], which is borderline metallic. The most general expression for the photoemission intensity involves the imaginary part of the Greens function. After a Fourier transform from k-space into real space, this becomes the electron propagator. It determines the amplitude of an electron to move from point A to point B, a
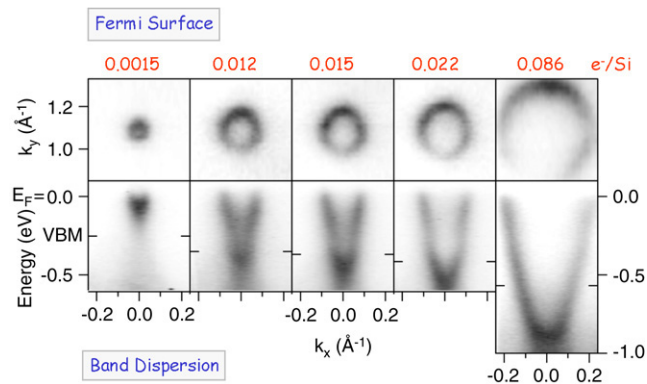

Fig. 7. Fermi surface (top) and band dispersion (bottom) of the two-dimensional Si(111) $\sqrt{3} \times \sqrt{3}$-Ag structure at various levels of doping with extra Ag atoms (in Si(111) monolayers, from [8]). The area of the Fermi circles increases with doping. The rigid band model breaks down at such high doping levels, as demonstrated by the downwards shift of the surface band minimum relative to the bulk valence band maximum (VBM, tickmarks). High photoemission intensity is shown dark in this and the following figures.
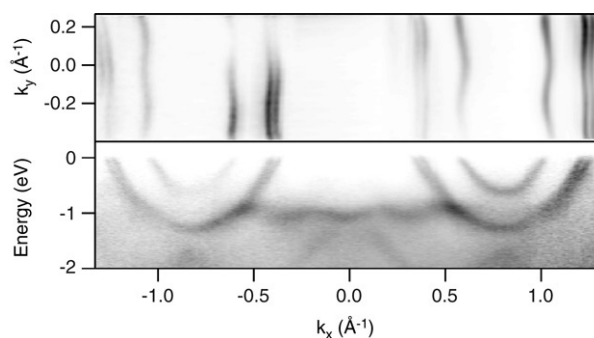

Fig. 8. Fermi surface (top) and band dispersion (bottom) of the Si(553)-Au chain structure (from [44]). In contrast to the 2D Fermi circles in Fig. 7, the Fermi surface is open and approaches straight lines in the 1D limit. Weak oscillations of the Fermi lines reveal the 2D/1D coupling ratio. It ranges from 1/10 to >1/70, the detection limit. A fractional band filling of 5/3 electrons per Au atom is obtained from the filled part of the Brillouin zone, assuming a spin-split band (see Figs. 9 and 10).

rather fundamental characterization of an electron moving in a solid.

In the following we will focus on determining the quantum numbers of two-and one-dimensional electrons by plotting the photoemission intensity I as a function of the three measurement parameters E, k_x, k_y. These can be grouped in two ways, either as band dispersion $I(E, k_x)$ or as Fermi surface $I(k_x, k_y)$. The band dispersion along the chain direction k_x is the more interesting part, since the perpendicular band dispersion vanishes in the one-dimensional limit. The difference between two- and one-dimensional Fermi surfaces is striking, as shown in Figs. 7 and 8. Two-dimensional Fermi surfaces are characterized by closed loops, such as the Fermi circles observed for the Si(111) $\sqrt{3} \times \sqrt{3}$-Ag structures doped by additional Ag atoms [8]. Chain structures have open Fermi surfaces consisting of oscillating lines along k_y (perpendicular to the chains). For a truly one-dimensional system the oscillations vanish, and one is left with straight lines through the Fermi points $\pm k_F$.

3.1. Two-dimensional electrons

In two dimensions, the band filling can be varied continuously by adding additional noble metal atoms to the semiconducting $\sqrt{3} \times \sqrt{3}$ monolayer structure of Ag and Au on Si(111), as shown in Fig. 3 (see [6,8,19–25]). The corresponding photoemission data in Fig. 7 clearly show Fermi circles, which expand with increasing doping by Ag atoms (beyond the 1 monolayer required for the semiconducting $\sqrt{3} \times \sqrt{3}$ structure). The number of doping-induced electrons per unit cell can be obtained from the area inside the Fermi circle, normalized to the surface Brillouin zone and multiplied by two (for spin up and down). The maximum amount of doping is reached for a $\sqrt{21} \times \sqrt{21}$ superlattice of doping atoms, where the Fermi surface contains 3 electrons per $\sqrt{21} \times \sqrt{21}$ unit cell ([8,21] and Fig. 3, orange symbols). Compared to bulk doping concentrations, these doping densities are huge. Already the first data point lies beyond the semiconductor–metal transition, as evidenced by the observation of a tiny Fermi circle. This transition is observed in bulk Si at a doping level of 3×10^{21} cm^{-3} [60]. Two-dimensional electrons at surfaces can serve as prototypes for exploring the high density limit of a two-dimensional electron gas (in particular Si(111) $\sqrt{3} \times \sqrt{3}$-Ag, Au [6,8,19–22], Si(111) $\sqrt{7} \times \sqrt{3}$-In [7], or InAs [26,27]).

At such high doping, the rigid band model breaks down. This can be seen in the $E(k)$ band dispersions of Fig. 7, where the bottom of the surface band moves relative to the bulk valence band maximum (VBM), which is the natural reference energy in a semiconductor (tickmarks). At small doping, the bottom of the surface band lies 0.3 eV above the VBM, and at high coverages it moves all the way down to 0.3 eV below the VBM (see Fig. 2 in [8] for details). With dopant concentrations of 1%, there are first indications of an impurity state interacting with the surface conduction band. The intensity minimum above the bottom of the surface band has been attributed to an avoided crossing with such an impurity state [8,22]. Another deviation from the free electron gas is the non-parabolic band dispersion at the bottom of the surface band. It becomes more V-shaped for low doping, similar to the π band in graphene, which has produced interesting new electron gas physics recently.

3.2. One-dimensional electrons

When going from two-dimensional structures to one-dimensional chains, the topology of the Fermi surface changes dramatically, as one can see from a comparison of Figs. 7 and 8. Closed Fermi circles become open surfaces consisting of undulating lines. The amplitude of the undulations is a measure of the residual two-dimensional coupling between the chains. It can be quantified by a tight binding calculation [44,45] which uses three couplings, two along the chains (t_1 and t_3 for first and second neighbor) and one between the chains (t_2). The coupling ratio t_1/t_2 for the data from the Si(553)-Au surface in Fig. 8 ranges from $t_1/t_2 = 39, 46$ for the doublet of Fermi lines with to $t_1/t_2 = 12$ for the single line. For structures with larger chain spacing, such as Si(557)-Au, the undulations of the Fermi lines become undetectable, which gives a lower limit $t_1/t_2 > 70$.
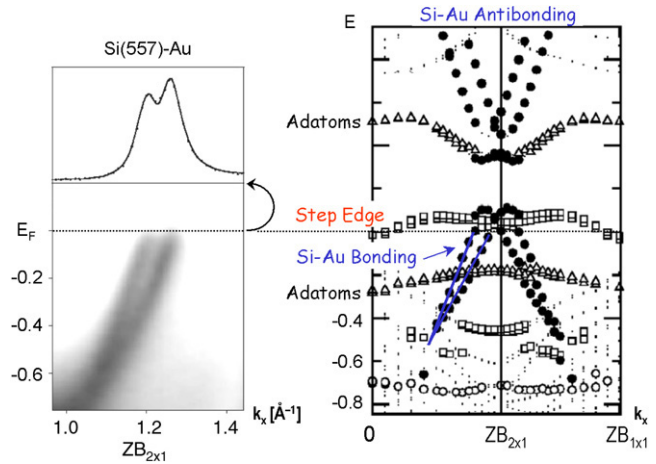

Fig. 9. Close-up of the two half-filled bands at the Si(557)-Au surface [41], compared to a first principles band calculation [54] which predicts a spin-split band caused by spin–orbit interaction with the Au atoms (Rashba effect). This assignment is confirmed experimentally in Fig. 10. The atomic chains assigned to various bands are shown in Fig. 4 (with the same colour code).

This rapid decay of the inter-chain coupling with increasing spacing is due to the exponential decay of the wave functions of the dangling bond states that form the half-filled bands. The decay constant is of the order of an atom diameter, while the chain spacing increases by almost two silicon atom diameters from Si(553)-Au to Si(557)-Au.

The observation of two closely-spaced bands in Figs. 8 and 9 [40,41,43] brings up an intriguing question: Could this be the sought-after spin–charge separation in a one-dimensional electron gas? Early photoemission work on Si(557)-Au proposed such an explanation [40]. However, the observation that the splitting remains at E_F rules out such an assignment [41,43]. This can be seen from the double-peaked momentum distribution at E_F in Fig. 9 (top left). The question remains, why the surface chooses two half-filled bands (corresponding to two broken bonds with one electron each), instead of pairing the two electrons. Theory has been very helpful in solving this riddle. A first principles density functional calculation [54] has been able to reproduce the two closely-spaced, half-filled bands after including relativistic effects (see Fig. 9, right). The surprising conclusion is that the bands are spin-split. Neither Si nor Au have any tendency to become magnetic. However, Au has a high atomic number Z, which generates a significant spin–orbit splitting. Combined with the lack of inversion symmetry at a surface, one obtains a spin splitting. This effect can be described by the Rashba Hamiltonian, which is proportional to $(\mathbf{n} \times \mathbf{p}) \cdot \boldsymbol{\sigma}$, a scalar combination of two vectors and a pseudovector ($\mathbf{n}$ is the surface normal, $\mathbf{p}$ the momentum operator, and $\boldsymbol{\sigma}$ the spin operator). Reversing the spin $\boldsymbol{\sigma}$ changes the sign of the interaction and leads to a spin splitting. Reversing both spin and momentum gives the same energy. The spin pattern at the Fermi surface consists of in-plane spins oriented parallel and antiparallel to the Fermi lines. Although each of the two bands is 100% spin-polarized, their combined spins vanish. There is no net magnetization at the surface.
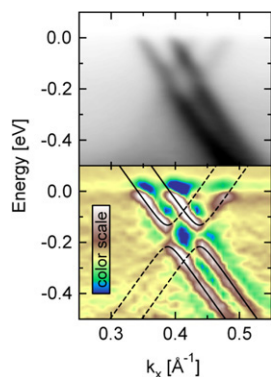
Fig. 10. Further zoom into the crossing between back-folded bands at $k_x = ZB_{2\times1}$ in Fig. 9, this time for the Si(553)-Au surface [49]. Two of the four band crossings are avoided, as one can see from the interruption of the bands in the second derivative (bottom panel). The avoided crossings are offset in **k** (horizontally), which shows that the band splitting is a spin splitting due to the spin–orbit interaction (Rashba effect). A ferromagnetic, antiferromagnetic, or unpolarized band splitting would have avoided crossings at the other two locations, which are offset in E (vertically).

The spin splitting has recently been confirmed experimentally by angle-resolved photoemission [49], as shown in Fig. 10. This figure is a further close-up in **k**-space from Fig. 9, zooming in onto the pattern of avoided crossings between the two bands and their back-folded counterparts at the 2×1 Brillouin zone boundary ($ZB_{2\times1}$). These measurements are for the Si(553)-Au surface, where the back-folding is easier to observe than on Si(557)-Au. Bands with opposite spin are able to cross each other, while bands with equal spin form an avoided crossing. Only a spin–orbit splitting gives the observed pattern, where the two avoided crossings are shifted in **k** (horizontally). They would have been shifted in E (vertically) for other common splittings, such as in ferromagnets, antiferromagnets, and nonmagnetic materials.

Doping of one-dimensional chain structures proceeds quite different from the two-dimensional case. Each chain structure automatically selects the optimum density of dopant atoms required for the lowest surface energy [55]. This leads to a well-defined density of Si dopants adsorbed on top of the chains or at the step edge. Typical densities range from 1/40 of a monolayer for Si(111) 5×2-Au (Fig. 6) down to <1/100 of a monolayer for the vicinal surfaces. There is little flexibility in altering the doping by changing the concentration of metal atoms. Nevertheless, different chain structures exhibit different band filling and thus allow for discrete variations of the electron density.

The chain structure with the highest observed dopant density is Si(111) 5×2-Au, which is shown in Fig. 6. The dopant atoms and the underlying 5×2 chains are brought out in panels (a) and (b), respectively, using different sample bias voltages for tunnelling into atom-specific orbitals. The Si dopants occupy a 5×4 lattice, but this lattice is only half-occupied. One can discern short sections of a few dopants in a row, which alternate with empty sections of the same length. This nanometer-scale phase separation of a chain into doped and undoped sections can be understood as the outcome of a competition between the optimum doping (which favours a 5×8 dopant

lattice [55]) and the Fermi surface nesting (which leads to a 5×4 periodicity [51]). The resulting compromise is a fifty-fifty combination of filled and empty 5×4 sections. These are the low-dimensional analogue of the stripes observed in the two-dimensional electron gas [5] and in high temperature superconductors. Again, there is a surprise: The doped regions are semiconducting, and the empty regions metallic (see [50]), opposite to the normal concept of doping in semiconductors and superconductors. The correlation between the doping atoms and their charge distribution can be inferred by comparing panel (a) with the dI/dV image in panel (c), which is proportional to the density of states. This particular tunneling energy ($E_F + 0.8$ eV) lies above the semiconducting gap, which extends from E_F to $E_F + 0.5$ eV. The states displaced from the band gap pile up at this energy and make the semiconducting regions appear bright.

An interesting fractional band filling [44] occurs for the Si(553)-Au surface in Fig. 8 (bottom). The two closely-spaced bands are a bit more than half-filled, and the filling of the single band is a bit less than one third. That brings the total filling very close to 5/3, taking into account that the two half-filled bands are spin split. At a first glance, the fractional filling is reminiscent of the fractional quantum Hall effect in the two-dimensional electron gas. However, there is no applied magnetic field in these photoemission experiments. Instead, the fractional filling can be explained by a tripling of the chain period at the step edge, where the dopants reside [44,45]. This tripling vanishes at the centre of the terrace, where the Au chain is located (compare Fig. 4). Therefore, each Au atom gets 1/3 of the doping electrons.

In addition to fractional band filling, the tripling of the period also causes a fractional charge at the end of an interrupted chain. This has been suggested for Si(553)-Au [48], by analogy to earlier work on polyacetylene chains with a doubled period and a prediction for a tripled period [61]. The end of a finite chain segment sustains a zero-dimensional state [47], which may be viewed as the analogue of a two-dimensional surface state on top a three-dimensional bulk.

One-dimensional chain structures exhibit several other interesting features that go beyond the scope of this brief overview, such as the formation of charge density waves at low temperatures [28–30,43,46–48,62], one-dimensional plasmons [63], anisotropic conductivity [64,65], and the use of atom chains as tracks for an atomic scale memory [66].

4. Summary and future directions

In summary, the self-assembly of metallic surface structures on semiconducting substrates provides a new playground for exploring the two- and one-dimensional electron gas at high densities. These structures combine the best of two worlds: The atoms are firmly locked to the surface, while the metallic electrons, are decoupled from the silicon substrate. There are no bulk states in the band gap to hybridize with. Atomic chain structures have been full of surprises, such as the graphitic Si ribbon that drives the structures one-dimensional, the incorporation of metal chains in the middle of the terrace and not at the step edge, self-doping by Si atoms which makes

the surface semiconducting instead of metallic, a fractional band filling, and a spin splitting that does not involve magnetic materials. We are just beginning to explore this new territory and can look forward to many more interesting discoveries during a deeper exploration.

First, there are several immediate questions to be answered. It is not clear yet, which chains support metallic electrons. A good candidate is the spin-split, half-filled band which is in good agreement with photoemission [40,41,43] and first principles calculations [54]. It originates from the zig-zag chain of Si orbitals pointing towards the Au chain (shown in dark blue in Fig. 4). However, scanning tunnelling spectroscopy finds the step edge to be metallic instead [67]. That seems to match a flat band straddling the Fermi level in the calculation (Fig. 9). However, such a band has not been found in photoemission. Two-photon photoemission data of the unoccupied states do not show it either [68].

A second question is the precise structure of the chains. Only the structure of the Si(557)-Au surface in Fig. 4 is supported by two total energy calculations [45,53] and a surface X-ray diffraction experiment [42], and only for this surface there is a reasonable agreement between band calculations and photoemission. For the other chain structures we have working models based on total energy minimization using up to a hundred trial structures. However, there are many options to attach extra Si atoms to the step edges, where they can always achieve the optimum bond length without introducing strain. Step structures remain a challenge for total energy minimization.

There are several natural extensions of this work. Spin chains are created by many rare earths on Si(111) (see [69] and references in [16]). They all form similar 5×2 chain structures, but their magnetic moment varies with the filling of the 4f shell. The 5d electron is magnetically coupled to the 4f electrons and might be able to introduce a magnetic anisotropy or magnetic ordering along the chains. By alloying metal atoms with different valence it might be possible to vary the band filling continuously, not just in discrete steps. The unoccupied part of the band structure is just beginning to be explored using two-photon photoemission [68]. This pump-probe technique also makes the dynamics of electrons in atomic chains accessible, down to the 50 fs time scale. Since the interaction between electrons is predicted to be much stronger in one dimension, one might expect radical changes in the decay mechanism of hot electrons.

Among the possibilities for further exploration there is one particularly fascinating path, i.e. applying a **B**-field in search of exotic states of matter, such as composites of electrons and magnetic flux quanta. However, the situation is different from the quantum Hall effect. Since the electron density is several orders of magnitude higher at surfaces, the density of flux quanta at realistic **B**-fields is much too low to match the electron density. In a one-dimensional gas, the character of Landau orbits is going to change dramatically, if they exist. Closed de Haas van Alphen orbits in reciprocal space cease to exist in 1D structures with open Fermi surfaces. Detailed calculations for anisotropic solids indicate a complex set of coupled surface

modes in the presence of a magnetic field [70]. Judging from the many surprises with one-dimensional chains, it may be best to just try it, without speculating too much about the results. Since photoemission is not possible in a strong **B**-field, scanning tunnelling spectroscopy (STS) is a natural technique. Quantum oscillations have been observed by STS in two-dimensional systems [71,72].

In order to explore spin–charge separation, it will be advantageous to scale up the electron–electron correlation by increasing the onsite Coulomb repulsion U_C. Photoemission experiments showing separate spinon and holon peaks were performed in highly-correlated systems with a substantial U_C and localized orbitals, such as C2p orbitals in the organic conductor TTF-TCNQ [73] and Cu3d orbitals in cuprates [74]. Model calculations suggest that a large U_C increases the energy scale for spinon–holon separation such that it becomes comparable to the bandwidth [73]. On semiconductor surfaces it is possible to increase U_C by an order of magnitude by choosing SiC substrates instead of Si [11–13]. All these possibilities show that we are just beginning to exploit the one-dimensional electron gas in atom chains. Many interesting avenues lie ahead.

Acknowledgments

References

[1] T. Ando, A.B. Fowler, F. Stern, Electronic properties of two-dimensional systems, Rev. Modern Phys. 54 (1983) 437.

[2] K. von Klitzing, The quantized Hall effect, Rev. Modern Phys. 58 (1986) 519.

[3] H.L. Störmer, D.C. Tsui, A.C. Gossard, The fractional quantum Hall effect, Rev. Modern Phys. 71 (1999) S298.

[4] R.B. Laughlin, Nobel lecture: Fractional quantization, Rev. Modern Phys. 71 (1999) 863.

[5] J.P. Eisenstein, Two-dimensional electrons in excited Landau levels: Evidence for new collective states, Solid State Commun. 117 (2001) 123.

[6] S. Hasegawa, X. Tong, S. Takeda, N. Sato, T. Nagao, Structures and electronic transport on silicon surfaces, Prog. Surf. Sci. 60 (1999) 89.

[7] E. Rotenberg, H. Koh, K. Rossnagel, H.W. Yeom, J. Schäfer, B. Krenzer, M.P. Rocha, S.D. Kevan, Indium $\sqrt{7} \times \sqrt{3}$ on Si(111): A nearly free electron metal in two dimensions, Phys. Rev. Lett. 91 (2003) 246404.

[8] J.N. Crain, M.C. Gallagher, J.L. McChesney, M. Bissen, F.J. Himpsel, Doping of a surface band on Si(111) $\sqrt{3} \times \sqrt{3}$-Ag, Phys. Rev. B 72 (2005) 045312.

[9] J. Ortega, F. Flores, A.L. Yeyati, Electron correlation effects in the Si(111)-7×7 surface, Phys. Rev. B 58 (1998) 4584.

[10] I. Barke, Fan Zheng, A.R. Konicek, R.C. Hatch, F.J. Himpsel, Electron–phonon interaction at the Si(111)-7×7 surface, Phys. Rev. Lett. 96 (2006) 216801.

[11] L.I. Johansson, F. Owman, P. Mårtensson, Surface state on the SiC(0001)-($\sqrt{3} \times \sqrt{3}$) surface, Surf. Sci. 360 (1996) L478.

[12] J.-M. Themlin, I. Forbeaux, V. Langlais, H. Belkhir, J.-M. Debever, Unoccupied surface states on the $\sqrt{3} \times \sqrt{3}R30°$ reconstruction of 6H-SiC(0001), Europhys. Lett. 39 (1997) 61.

[13] V. Ramachandran, R.M. Feenstra, Scanning tunneling spectroscopy of Mott–Hubbard states on the 6H-SiC(0001) $\sqrt{3} \times \sqrt{3}$ Surface, Phys. Rev. Lett. 82 (1999) 1000.

[14] A.R. Goñi, A. Pinczuk, J.S. Weiner, J.M. Calleja, B.S. Dennis, L.N. Pfeiffer, K.W. West, One-dimensional plasmon dispersion and dispersionless intersubband excitations in GaAs quantum wires, Phys. Rev. Lett. 67 (1991) 3298.

[15] O.M. Auslaender, H. Steinberg, A. Yacoby, Y. Tserkovnyak, B.I. Halperin, K.W. Baldwin, L.N. Pfeiffer, K.W. West, Spin–charge separation and localization in one dimension, Science 308 (2005) 88.

[16] J.N. Crain, F.J. Himpsel, Low-dimensional electronic states at silicon surfaces, Appl. Phys. A 82 (2006) 431.

[17] T. Giamarchi, Quantum Physics in One Dimension, Oxford University Press, New York, 2004.

[18] M.G. Zacher, E. Arrigoni, W. Hanke, J.R. Schrieffer, Systematic numerical study of spin–charge separation in one dimension, Phys. Rev. B 57 (1998) 6370.

[19] R.I.G. Uhrberg, H.M. Zhang, T. Balasubramanian, et al., Photoelectron spectroscopy study of Ag/Si(111) $\sqrt{3} \times \sqrt{3}$ and the effect of additional Ag adatoms, Phys. Rev. B 65 (2002) 081305.

[20] J.N. Crain, K.N. Altmann, C. Bromberger, F.J. Himpsel, Fermi surfaces of surface states on Si(111)-Ag, Au, Phys. Rev. B 66 (2002) 205302.

[21] I. Matsuda, T. Hirahara, M. Konishi, C. Liu, H. Morikawa, M. D'Angelo, S. Hasegawa, T. Okuda, T. Kinoshita, Evolution of Fermi surface by electron filling into a free-electronlike surface state, Phys. Rev. B 71 (2005) 235315.

[22] C. Liu, I. Matsuda, R. Hobara, S. Hasegawa, Interaction between adatom-induced localized states and a Quasi-two-dimensional electron gas, Phys. Rev. Lett. 96 (2006) 036803.

[23] Y.G. Ding, C.T. Chan, K.M. Ho, Structure of the $(\sqrt{3} \times \sqrt{3})R30°$ Ag/Si(111) surface from first-principles calculations, Phys. Rev. Lett. 67 (1991) 1454; Phys. Rev. Lett. 69 (1992) 2452.

[24] H. Aizawa, M. Tsukada, First-principles study of Ag adatoms on the Si(111)-$\sqrt{3} \times \sqrt{3}$-Ag surface, Phys. Rev. B 59 (1999) 10923.

[25] L. Chen, H.J. Xiang, B. Li, A. Zhao, X. Xiao, J. Yang, J.G. Hou, Q. Zhu, Detecting surface resonance states of Si(111)-$\sqrt{3}\sqrt{3}$-Ag with a scanning tunneling microscope, Phys. Rev. B 70 (2004) 245431.

[26] L.O. Olsson, C.B.M. Andersson, M.C. Hakansson, J. Kanski, L. Ilver, U.O. Karlsson, Charge accumulation at InAs surfaces, Phys. Rev. Lett. 76 (1996) 3626.

[27] V.Yu. Aristov, V.M. Zhilin, C. Grupp, A. Taleb-Ibrahimi, H.J. Kim, P.S. Mangat, P. Soukiassian, G. Le Lay, Photoemission measurements of quantum states in accumulation layers at narrow band gap III–V semiconductor surfaces, Appl. Surf. Sci. 166 (2000) 263.

[28] H.W. Yeom, S. Takeda, E. Rotenberg, I. Matsuda, K. Horikoshi, J. Schaefer, C.M. Lee, S.D. Kevan, T. Ohta, T. Nagao, S. Hasegawa, Instability and charge density wave of metallic quantum chains on a silicon surface, Phys. Rev. Lett. 82 (1999) 4898.

[29] J.R. Ahn, J.H. Byun, H. Koh, E. Rotenberg, S.D. Kevan, H.W. Yeom, Mechanism of gap opening in a triple-band peierls system: In atomic wires on Si, Phys. Rev. Lett. 93 (2004) 106401.

[30] C. Gonzales, F. Flores, J. Ortega, Soft phonon, dynamical fluctuations, and a reversible phase transition: Indium chains on silicon, Phys. Rev. Lett. 96 (2006) 136101.

[31] E.D. Williams, R.J. Phaneuf, J. Wei, N.C. Bartelt, T.L. Einstein, Thermodynamics and statistical mechanics of the faceting of stepped Si(111), Surf. Sci. 294 (1993) 219.

[32] J. Viernow, J.L. Lin, D.Y. Petrovykh, F.M. Leibsle, F.K. Men, F.J. Himpsel, Regular step arrays on silicon, Appl. Phys. Lett. 72 (1998) 948.

[33] J.L. Lin, D.Y. Petrovykh, J. Viernow, F.K. Men, D.J. Seo, F.J. Himpsel, J. Appl. Phys. 84 (1998) 255.

[34] Y.N. Yang, E.S. Fu, E.D. Williams, An STM study of current-induced step bunching on Si(111), Surf. Sci. 356 (1996) 101.

[35] S. Yoshida, T. Sekiguchi, K.M. Itoh, Atomically straight steps on vicinal Si(111) surfaces prepared by step-parallel current in the kink-up direction, Appl. Phys. Lett. 87 (2005) 031903.

[36] A. Kirakosian, R. Bennewitz, J.N. Crain, T. Fauster, J.L. Lin, D.Y. Petrovykh, F.J. Himpsel, Atomically accurate Si grating with 5.73 nm period, Appl. Phys. Lett. 79 (2001) 1608.

[37] F.J. Himpsel, A. Kirakosian, J.N. Crain, J.-L. Lin, D.Y. Petrovykh, Self-assembly of one-dimensional nanostructures at silicon surfaces, Solid State Commun. 117 (2001) 149.

[38] M. Jalochowski, M. Strozak, R. Zdyb, Gold-induced ordering on vicinal Si(111), Surf. Sci. 375 (1997) 203.

[39] A.A. Baski, K.M. Saoud, K.M. Jones, 1-D nanostructures grown on the Si(5 5 12) surface, Appl. Surf. Sci. 182 (2001) 216.

[40] P. Segovia, D. Purdie, M. Hengsberger, Y. Baer, Observation of spin and charge collective modes in one-dimensional metallic chains, Nature 402 (1999) 504.

[41] R. Losio, K.N. Altmann, A. Kirakosian, J.-L. Lin, D.Y. Petrovykh, F.J. Himpsel, Band splitting for Si(557)-Au: Is it spin–charge separation? Phys. Rev. Lett. 86 (2001) 4632.

[42] I.K. Robinson, P.A. Bennett, F.J. Himpsel, Structure of quantum wires in Au/Si(557), Phys. Rev. Lett. 88 (2002) 096104.

[43] J.R. Ahn, H.W. Yeom, H.S. Yoon, I.W. Lyo, Metal-insulator transition in Au atomic chains on Si with two proximal bands, Phys. Rev. Lett. 91 (2003) 196403.

[44] J.N. Crain, K.N. Altmann, C. Bromberger, S.C. Erwin, A. Kirakosian, J.L. McChesney, J.-L. Lin, F.J. Himpsel, Fractional band filling in an atomic chain structure, Phys. Rev. Lett. 90 (2003) 176805.

[45] J.N. Crain, J.L. McChesney, F. Zheng, M.C. Gallagher, P.C. Snijders, M. Bissen, C. Gundelach, S.C. Erwin, F.J. Himpsel, Chains of gold atoms with tailored electronic states, Phys. Rev. B 69 (2004) 125401.

[46] J.R. Ahn, P.G. Kang, K.D. Ryang, H.W. Yeom, Coexistence of two different peierls distortions with an atomic scale wire: Si(553)-Au, Phys. Rev. Lett. 95 (2005) 196402.

[47] J.N. Crain, D.T. Pierce, End states in one-dimensional atom chains, Science 307 (2005) 703.

[48] P.C. Snijders, S. Rogge, H.H. Weitering, Competing periodicities in fractionally filled one-dimensional bands, Phys. Rev. Lett. 96 (2006) 076801.

[49] I. Barke, Fan Zheng, T.K. Rügheimer, F.J. Himpsel, Experimental evidence for spin-split bands in a one-dimensional chain structure, Phys. Rev. Lett. 97 (2006) 226405.

[50] H.S. Yoon, S.J. Park, J.E. Lee, C.N. Whang, I.W. Lyo, Novel electronic structure of inhomogeneous quantum wires on a Si surface, Phys. Rev. Lett. 92 (2004) 096801.

[51] J.L. McChesney, J.N. Crain, V. Pérez-Dieste, Fan Zheng, M.C. Gallagher, M. Bissen, C. Gundelach, F.J. Himpsel, Electronic stabilization of a 5 × 4 dopant superlattice on Si(111) 5 × 2-Au, Phys. Rev. B 70 (2004) 195430.

[52] S.C. Erwin, H.H. Weitering, Theory of the honeycomb chain-channel reconstruction of M/Si(111)-(3 × 1), Phys. Rev. Lett. 81 (1998) 2296.

[53] D. Sanchez-Portal, J.D. Gale, A. Garcia, R.M. Martin, Two distinct metallic bands associated with monatomic Au wires on the Si(557)-Au surface, Phys. Rev. B 65 (2002) 081401.

[54] D. Sanchez-Portal, S. Riikonen, R.M. Martin, Role of spin–orbit splitting and dynamical fluctuations in the Si(557)-Au surface, Phys. Rev. Lett. 93 (2004) 146803.

[55] S.C. Erwin, Self-doping of gold chains on silicon: A new structural model for Si(111)-(5 × 2)-Au, Phys. Rev. Lett. 91 (2003) 206101.

[56] Y.-W. Son, M.L. Cohen, G.G. Louie, Energy gaps in graphene nanoribbons, Phys. Rev. Lett. 97 (2006) 216803.

[57] F.J. Himpsel, Angle-resolved measurements of the photoemission of electrons in the study of solids, Adv. Phys. 32 (1983) 1.

[58] S.D. Kevan (Ed.), Angle-Resolved Photoemission, Elsevier, Amsterdam, 1992.

[59] Neville Smith, Science with soft X-rays, Phys. Today 54 (2001) 29.

[60] D.E. Eastman, P. Heimann, F.J. Himpsel, B. Reihl, D.M. Zehner, C.W. White, Electronic properties of laser-annealed Si(111)-(1 × 1) surfaces of highly doped silicon, Phys. Rev. B 24 (1981) 3647.

[61] W.P. Su, J.R. Schrieffer, A.J. Heeger, Soliton excitations in polyacetylene, Phys. Rev. B 22 (1980) 2099; W.P. Su, J.R. Schrieffer, Fractionally charged excitations in charge-density-wave systems with commensurability 3, Phys. Rev. Lett. 46 (1981) 738.

[62] T. Nagao, S. Yaginuma, T. Inaoka, T. Sakurai, One-dimensional plasmon in an atomic-scale metal wire, Phys. Rev. Lett. 97 (2006) 116802.

[63] G. Lee, J.D. Guo, E.W. Plummer, Real-space observation of nanoscale inhomogeneities and fluctuations in a phase transition of a surface quasi-one-dimensional system: In/Si(111), Phys. Rev. Lett. 95 (2005) 116103.

[64] T. Tanikawa, I. Matsuda, T. Kanagawa, S. Hasegawa, Surface-state electrical conductivity at a metal–insulator transition on silicon, Phys. Rev. Lett. 93 (2004) 016801.

[65] C. Tegenkamp, Z. Kallassy, H. Pfnür, H.-L. Günter, V. Zielasek, M. Henzler, Switching between one and two dimensions: Conductivity of Pb-induced chain structures on Si(557), Phys. Rev. Lett. 95 (2005) 176804.

[66] R. Bennewitz, J.N. Crain, A. Kirakosian, J.-L. Lin, J.L. McChesney, D.Y. Petrovykh, F.J. Himpsel, Atomic scale memory at a silicon surface, Nanotechnology 13 (2002) 499.

[67] H.W. Yeom, J.R. Ahn, H.S. Yoon, I.-W. Lyo, H. Jeong, S. Jeong, Real-space investigation of the metal–insulator transition of Si(557)-Au, Phys. Rev. B 72 (2005) 035323.

[68] T.K. Rügheimer, Th. Fauster, F.J. Himpsel, Unoccupied electronic states in atomic chains on Si(557)-Au: Time-resolved two-photon photoemission investigation, Phys. Rev. B 75 (2007) 121401(R).

[69] A. Kirakosian, J.L. McChesney, R. Bennewitz, J.N. Crain, J.-L. Lin, F.J. Himpsel, One-dimensional Gd-induced chain structures on Si(111) surfaces, Surf. Sci. 498 (2002) L109.

[70] R.F. Wallis, J.J. Brion, E. Burstein, A. Hartstein, Theory of surface polaritons in anisotropic dielectric media with application to surface magnetoplasmons in semiconductors, Phys. Rev. B 9 (1974) 3424.

[71] D. Haude, M. Morgenstern, I. Meinel, R. Wiesendanger, Local density of states of a three-dimensional conductor in the extreme quantum limit, Phys. Rev. Lett. 86 (2001) 1582.

[72] T. Matsui, H. Kambara, Y. Niimi, K. Tagami, M. Tsukada, H. Fukuyama, STS observations of landau levels at graphite surfaces, Phys. Rev. Lett. 94 (2005) 226403.

[73] R. Claessen, M. Sing, U. Schwingenschlögl, P. Blaha, M. Dressel, C.S. Jacobsen, Spectroscopic signatures of spin–charge separation in the Quasi-one-dimensional organic conductor TTF-TCNQ, Phys. Rev. Lett. 88 (2002) 096402.

[74] B.J. Kim, H. Koh, E. Rotenberg, S.-J. Oh, H. Eisaki, N. Motoyama, S. Uchida, T. Tohyama, S. Maekawa, Z.-X. Shen, C. Kim, Distinct spinon and holon dispersions in photoemission spectral functions from one-dimensional $SrCuO_2$, Nat. Phys. 2 (2006) 397.